The Cationic Cell-Penetrating Peptide CPP^{TAT} Derived from the HIV-1 Protein TAT Is Rapidly Transported into Living Fibroblasts: Optical, Biophysical, and Metabolic Evidence†

André Ziegler,‡ Pierluigi Nervi,‡ Markus Dürrenberger,§ and Joachim Seelig*,‡

Department of Biophysical Chemistry and Center of Microscopy, Biozentrum, University of Basel, Klingelbergstrasse 70, CH-4056 Basel, Switzerland

Received April 26, 2004; Revised Manuscript Received September 17, 2004

ABSTRACT: Cell-penetrating peptides (CPPs) are cationic peptides which, when linked to genes, proteins, or nanoparticles, facilitate the transport of these entities across the cell membrane. Despite their potential use for gene transfer and drug delivery, the mode of action of CPPs is still mysterious. It has even been argued that the observed transport across the cell membrane is an artifact caused by chemical fixation of the cells, a common preparation method for microscopic observation. Here we have synthesized a fluorescent derivative of the HIV-1 TAT protein transduction domain [Fg-CPP$^{TAT(PTD)}$] and have observed its uptake into nonfixated living fibroblasts with time-lapse confocal microscopy, eliminating the need for fixation. We observe that Fg-CPP$^{TAT(PTD)}$ enters the cytoplasm and nucleus of nonfixated fibroblasts within seconds, arguing against the suggested artifact of cell fixation. Using differential interference contrast microscopy, dense aggregates are detected on the cell surface. Several observations suggest that these aggregates consist of Fg-CPP$^{TAT(PTD)}$ bound to membrane-associated heparan sulfate (HS). The aggregates grow in parallel with Fg-CPP$^{TAT(PTD)}$ uptake and are detected only on fibroblasts showing Fg-CPP$^{TAT(PTD)}$ uptake. These observations resemble earlier reports of "capping" of cell surface molecules combined with a polarized endocytotic flow. Enzymatic removal of extracellular HS reduced the rate of both Fg-CPP$^{TAT(PTD)}$ uptake and aggregate formation, demonstrating that HS is involved in the uptake mechanism. The functionality of the fibroblasts during the CPP uptake was investigated with a cytosensor microphysiometer measuring the extracellular acidification rate (ECAR). Short exposures (2.5 min) to the CPP reduced the ECAR which was, however, reversible upon reperfusion with buffer only. In contrast, no recovery to baseline values was observed after repeated exposures to the CPP, suggesting that the CPP is toxic in long-term applications.

In 1965, it was observed that histones and cationic polyamines such as polylysine stimulate the uptake of albumin by tumor cells in culture (*1*, *2*). In this early study, the albumin was not covalently bound to the uptake promoters. It was then found that direct conjugation of albumin and other proteins to polylysine made the transport of these proteins more specific and more effective (*3*). A systematic comparison of different homopolymers of cationic amino acids further revealed that medium-length polymers of arginine were significantly more effective at entering cells than were similar-length polymers composed of lysine, ornithine, or histidine (*4*).

Following a completely different line of research, it was discovered in 1988 that a natural polycationic protein, the trans-acting activator of transcription (TAT)[1] of the human immunodeficiency virus (HIV-1), also passed very efficiently through cell membranes of cultured mammalian cells (*5*, *6*). Covalently binding the TAT protein [or a specific peptide sequence of it (*7*)] to proteins (*8*) or fluorescent markers (*9*) allowed these molecules to traverse the cell membrane. Following this discovery, additional polycationic peptides of natural (vp22 and AntP) and synthetic origin (transportan) have been identified which also facilitate cellular uptake, alone or together with attached cargos such as genes, proteins, or even nanoparticles. These peptide sequences were named alternatively protein transduction domains (PTDs) (*10*), cell-penetrating peptides (CPPs) (*11*) or Trojan horse peptides (*12*). Polylysine was however not included in this class of compounds (*4*, *11*, *12*).

The mechanism for the CPP-facilitated cellular uptake is unknown (*10*, *13*). The common characteristic of all CPPs and polylysine is the high density of basic amino acid residues (Arg and Lys). The large charge at physiological pH excludes the passive diffusion of CPPs across the lipid

† This work was supported by Swiss National Science Foundation Grant 31-58800.99.

* To whom correspondence should be addressed. Telephone: +41-61-267 2190. Fax: +41-61-267 2189. E-mail: joachim.seelig@unibas.ch.

‡ Department of Biophysical Chemistry.

§ Center of Microscopy.

[1] Abbreviations: CPP, cell-penetrating peptide; CPP$^{TAT(PTD)}$, PTD sequence (YGRKKRRQRRR) of HIV-1 TAT; DIC, differential interference contrast; DMEM, Dulbecco's modified Eagle's medium; ECAR, extracellular acidification rate; Fg, fluorescent FITC bound to a spacer pentapeptide [(βA)GGGG]; Fg-CPP$^{TAT(PTD)}$, fluorescent peptide Fg linked to CPP$^{TAT(PTD)}$; FITC, fluorescein isothiocyanate; HIV, human immunodeficiency virus; HS, heparan sulfate; ITC, isothermal titration calorimetry; PTD, protein transduction domain; TAT, trans-acting activator of transcription.

10.1021/bi0491604 CCC: $30.25
Published on Web 12/15/2004

bilayer. Classical uptake mechanisms such as protein-based receptors and transporters appear not to be involved (*14*) since D-isomers of CPPs exhibit the same transduction efficiency as the naturally occurring L-amino acid sequences (*15*). Classical endocytosis as an uptake mechanism is controversial. In a number of reports, CPP uptake was not inhibited at 4 °C (*4*, *7*, *14*, *16*) or in the presence of inhibitors of endocytosis (*7*); in contrast, capture of CPPs in endocytotic vesicles was observed when *soluble* heparan sulfate was added (*17*). The need for membrane-attached HS in CPP uptake was negated in an early publication (*9*), but became substantiated in subsequent studies (*7*, *18*−*20*). Recently, it has been postulated that the membrane translocation of CPPs could even be an artifact of the chemical fixation prior to microscopic observation (*21*).

Despite the controversy and uncertainties surrounding the translocation mechanism, the cell penetrating property of these peptides makes them an attractive vector for promoting the cellular uptake of covalently bound genes, proteins, drugs, and 200 nm-sized imaging reagents (*10*). There is widespread hope that these peptides might be used in medicine and biotechnology to increase the rate of cellular uptake of problematic drugs and to increase the efficiency of gene therapies using nonviral vectors (*10*).

For biomedical applications in humans, however, little is known about whether these vectors cause morphological alterations or exert toxic effects on mammalian cells. For example, the TAT peptide (82 amino acid residues) is neurotoxic, and residues 31−61 have been identified as being responsible for this neurotoxicity (*22*). In contrast, residues 48−85, containing also the minimum sequence required for the membrane translocation [residues 47−57; termed the TAT protein transduction domain, TAT(PTD) (*8*)], are not neurotoxic (*22*). As far as the 11-amino acid TAT(PTD) sequence is concerned, only two studies have investigated its toxicity with respect to cell cultures (*7*, *23*). Both studies could not identify acute cytotoxic effects of the peptide at concentrations of 20 (*23*) or 100 μM (*7*) and exposure times of up to 30 min. At longer exposure times (24 h), however, TAT caused cell necrosis in 60% of the cells (*7*) so that only short-term exposures seem to be practical for cellular drug import and gene transfection in biotechnology.

In the study presented here, we report that even shorter TAT(PTD) exposures (<4 min) lead to functional alterations of living fibroblasts. The rapid uptake of TAT(PTD) into living fibroblasts with intact cell membranes was observed and is thus not an artifact of chemical fixation. Several observations indicate that aggregation of the cell surface glycosaminoglycan heparan sulfate (HS) is an important element in the uptake mechanism.

EXPERIMENTAL PROCEDURES

Peptide Synthesis. Peptide synthesis of TAT(PTD) (H_3N^+-YGRKKRRQRRR-COO^-), g [H_3N^+-(βA)GGGG-COO^-], and g-$CPP^{TAT(PTD)}$ [H_3N^+-(βA)GGGGYGRKKRRQRRR-COO^-] was performed on a solid-phase resin using an Abimed EPS221 peptide synthesizer (Langenfeld) (*24*). Before removal of the resin and protection groups from the peptide, g-$CPP^{TAT(PTD)}$ and g were linked covalently at the amino end to fluorescein isothiocyanate (FITC, F) via a thiourea bond (*25*). β-Alanine (βA) was required to prevent the loss of FITC during the subsequent removal of the resin and protection groups using trifluoroacetic acid. Thereafter, the peptides were purified by preparative high-pressure liquid chromatography. The masses of TAT(PTD) (1560.8 Da), Fg (704.7 Da), and Fg-$CPP^{TAT(PTD)}$ (2247.5 Da) were confirmed by electrospray ionization mass spectrometry. Peptide purity (>97%) was assessed by analytical HPLC.

Materials. Heparan sulfate, sodium salt [fraction I (*26*), average molecular mass of 14 200 Da, sulfate content of 6.44%] was from Celsus Laboratories (Cincinnati, OH). Heparinase III and all other HPLC-grade chemicals were from Fluka (Buchs, Switzerland).

Cell Line. Mouse embryo fibroblasts (NIH 3T3) were used in all experiments. Cells were cultured in Dulbecco's modified Eagle's medium (DMEM) supplemented with 10% (v/v) calf serum, 0.3 g/L L-glutamine, 100 units/mL penicillin, and 100 units/mL streptomycin, and were incubated in humidified CO_2 containing (5%) air at 37 °C.

Confocal Laser Scanning Microscopy. Fibroblasts were seeded in six-well dishes onto sterile noncoated microscopic cover slips and incubated for 48 h to obtain a confluency of ∼40−60%. Cover slips were mounted upside down on top of a custom-made microscopic perfusion chamber (volume of ∼0.25 mL), allowing the simultaneous image acquisition during the injection of labeled peptides. The infusion chamber initially contained DMEM with the fluorescent peptide, and the cells were imaged after the indicated contact time. For the kinetic studies, the fluorescent peptide (or heparan sulfate) was injected into DMEM. Here, the time for homogeneous mixing was approximately 10 s. Confocal images were acquired using a Leica TCS-NT-SP1 scanning system mounted on an inverted DMIRBE microscope (Leica Microsystems) with a PL APO 40×/NA 0.85 lens (Leica Microsystems) using a 2 s sample interval and an image resolution of 1024 data points for each lateral dimension of 250 μm. The detection pinhole diameter was set to 1.0 times the diameter of the Airy Disk, resulting in a thickness of the optical sections of 0.7 μm. Monochromatic argon laser (488 nm) excitation was used for the excitation of FITC. The offset and gain of the photomultiplier (8 bit resolution) were set to 0 and 200 for 0 and 100 μM Fg-$CPP^{TAT(PTD)}$, respectively. The recorded fluorescence intensity was plotted using a false-color green scale. For quantitative assessments, Fg-$CPP^{TAT(PTD)}$ was considered to be incorporated into fibroblasts when the average image intensity of a fibroblast increased by more than 10 units on an image intensity scale of 256 units. Detection with a FITC and TRITC filter (emission bands of 503−533 and 582−622 nm, respectively) was used for simultaneous measurements of FITC and propidium iodide.

Cytosensor Measurements of the TAT-Treated Cells. Fibroblasts were seeded on porous (3 μm pores) polycarbonate membranes (Corning, Cambridge, MA) and incubated for 48 h. Cells adhering to the polycarbonate membranes at a cell density of $0.5-1 \times 10^6$ cells/cm^2 were placed in eight parallel microflow chambers and positioned above a pH-sensitive sensor (Cytosensor microphysiometer, Molecular Devices, Sunnyvale, CA), which detects changes in extracellular pH (*27*, *28*). Here, fibroblasts were superfused at a rate of 120 μL/min with running medium (bicarbonate-free DMEM) at pH 7.40 and 37 °C. Every 2 min, the flow of running medium was stopped for 20 s, during which time the extracellular acid accumulated. Measurements of the

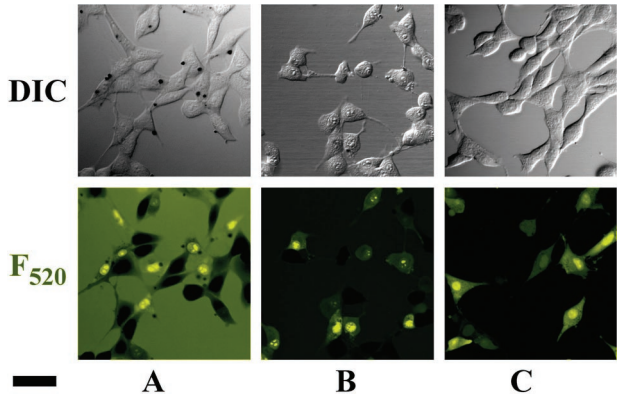

FIGURE 1: Optical evidence for uptake of the CPP into living fibroblasts. Mouse fibroblasts were cultured on uncoated cover slips and mounted upside down on top of a microscopic perfusion chamber containing 0.25 mL of the fluorescent Fg-CPP$^{TAT(PTD)}$ (100 μM). Confocal laser scanning microscopy of the differential interference contrast (DIC, top panel) and the fluorescent signal at 520 nm (F520, bottom panel) (bar = 50 μm). (A) After a 4 min period of contact with the peptide, the cells were imaged. The fluorescent Fg-CPP$^{TAT(PTD)}$ was found in the cytoplasm and nucleus of approximately half of the fibroblasts. In addition, formation of dark spots was observed on the cell membrane of those cells that incorporated the CPP (DIC images). (B) After a 4 min period of contact with Fg-CPP$^{TAT(PTD)}$ (100 μM), heparan sulfate was added [HS:Fg-CPP$^{TAT(PTD)}$ molar ratio $\sim$ 0.16], and the cells were imaged 2 min later. As a result of HS addition, the fluorescence of the extracellular Fg-CPP$^{TAT(PTD)}$ was quenched, whereas the intracellular Fg-CPP$^{TAT(PTD)}$ remained bright, yielding a better visualization of intracellular Fg-CPP$^{TAT(PTD)}$. On the other hand, the spots in the DIC image disappeared. (C) After a 4 min period of contact with Fg-CPP$^{TAT(PTD)}$ (100 μM), the cells were rinsed three times with 0.5 mL of regular DMEM to remove the excess fluorescent peptide in the extracellular space, and imaged 2 min later. Intracellular Fg-CPP$^{TAT(PTD)}$ is more visible than in panels A and B. On the other hand, the spots in the DIC image disappeared.

extracellular acidification rate (ECAR) were obtained by linear least-squares fit to the slope of the pH change (*27*). ECARs were in the range of 0.1 milli-pH unit/min. To compensate for small changes in cell densities, acidification rates were normalized (*27*) to 100% relative to the ECAR immediately before the superfusion with the test compounds [CPP$^{TAT(PTD)}$, amino acid monomers, and/or heparan sulfate].

In Vitro Measurement of Binding Parameters. The binding of Fg-CPP$^{TAT(PTD)}$ to heparan sulfate was assessed *in vitro* by static right-angle light scattering, fluorescence quenching, and high-sensitivity isothermal titration calorimetry as described previously (*29*).

RESULTS

TAT(PTD) Enters Living Cells Having Intact Membranes. When living fibroblasts were placed for 4 min in a cell culture medium containing the fluorescent cell-penetrating peptide Fg-CPP$^{TAT(PTD)}$ and imaged directly within this cell culture medium using confocal fluorescence microscopy, approximately half of the cells showed uptake of the CPP by the cytoplasm and nucleus (Figure 1A, F520). In this confocal imaging plane, the intracellular fluorescent CPP could be clearly distinguished from the extracellular CPP without chemical fixation of the cells or removal of the extracellular CPP. The CPP uptake was evident as some cells became clearly fluorescent, whereas other cells remained dark. In addition, those cells that incorporated the CPP showed formation of one, or sometimes two, dark spots on their cell membrane (Figure 1A, DIC).

After a 4 min contact time with the CPP, heparan sulfate (HS) was added [HS:Fg-CPP$^{TAT(PTD)}$ molar ratio of $\sim$0.16], and the cells were imaged 2 min later. As a result of the HS addition, the fluorescence of the extracellular CPP was quenched, whereas the intracellular CPP still remained bright, thus yielding a better visualization of the intracellular CPP (Figure 1B, F520) compared to the direct observation (Figure 1A). On the other hand, the dark aggregates on the membrane disappeared (Figure 1B, DIC), but some smaller aggregates appeared in the cell culture medium (see below).

The uptake of the CPP into living fibroblasts could be further demonstrated by removing the cover slip containing the fibroblasts from the microscope after the 4 min contact time with the CPP, washing it several times with regular cell culture medium to remove the extracellular Fg-CPP$^{TAT(PTD)}$, and observing the same cells immediately thereafter (Figure 1C). Again, approximately half of the cells showed uptake of the CPP, but the dark spots on the membrane had disappeared as a consequence of the washing procedure.

The integrity of the membrane before application of the CPP was confirmed with addition of propidium iodide, a marker that cannot cross an intact plasma membrane. Figure 2B (left panel) demonstrates that propidium iodide is excluded by almost all of the cells, demonstrating an impermeable cell membrane. However, the same cells that resisted the uptake of propidium iodide clearly showed an incorporation of Fg-CPP$^{TAT(PTD)}$ (Figure 2C, left panel). The integrity of the cell membrane was further evidenced by the fluorescent marker peptide Fg; i.e., the same fluorescent moiety used in the previous experiments (Figure 1), this time, however, not conjugated to the CPP. The fluorescent peptide Fg alone was not taken up by living fibroblasts (Figure 2B, right panel) unless it was covalently bound to the cell-penetrating peptide CPP$^{TAT(PTD)}$ (Figure 2C, right panel).

In the following, we were interested in the kinetics of Fg-CPP$^{TAT(PTD)}$ uptake, the nature of the dark spots observed in the DIC images, and the viability of the cells after the administration of the CPP.

Aggregates at the Surface of Cells with Fg-CPP$^{TAT(PTD)}$ Uptake and Their Relation to Heparan Sulfate. A comparison of the DIC image (Figure 1A, top) with the fluorescence image (Figure 1A, bottom) shows that those fibroblasts that incorporated Fg-CPP$^{TAT(PTD)}$ carry one, and also in a few instances two, characteristic dark spots on their cell membrane. The specific characteristics of the DIC (*30*) suggest that these dark spots are caused by dense aggregates. Rinsing the cells several times with regular cell medium (Figure 1C) or adding an external source of heparan sulfate removed these spots after 2 min (Figure 1B).

Heparan sulfate (HS) is a biological polysaccharide attached to several membrane proteins. It has been recently shown that the binding of HS to CPP$^{TAT(PTD)}$ leads to formation of aggregates, at least *in vitro* (*29*). This result suggests that the dark spots on the cell membrane (Figure 1) also represent aggregates of Fg-CPP$^{TAT(PTD)}$ bound to membrane-associated HS. This hypothesis was tested by adding external HS to living fibroblasts after a first exposure to Fg-CPP$^{TAT(PTD)}$. Under these conditions, aggregates were detected not only on the cell membrane (Figure 3A) but also

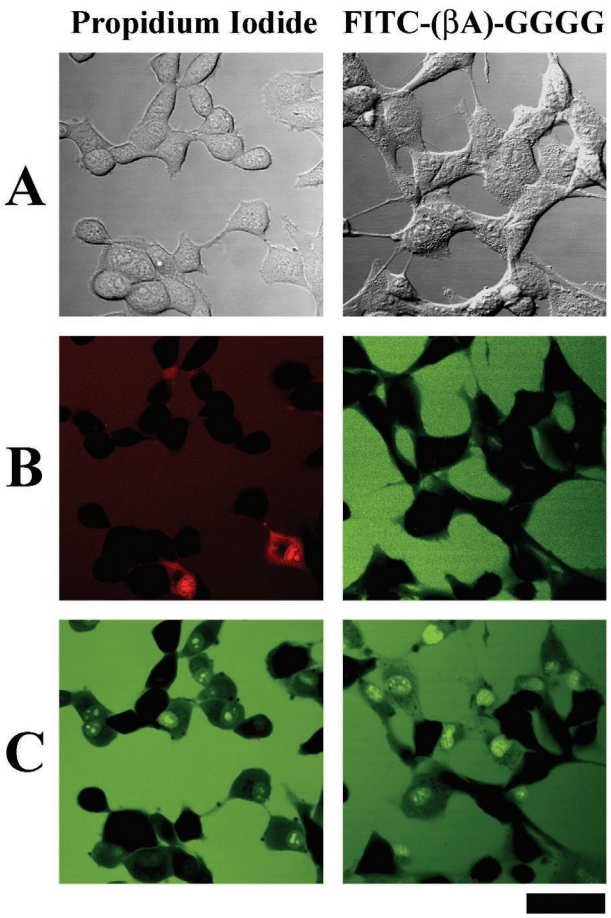

FIGURE 2: Plasma membrane integrity of the living fibroblasts. Membrane integrity is tested by exclusion of propidium iodide (left panel) and by exclusion of the fluorescent fragment Fg alone (right panel). The left panel shows the resistance to propidium iodide. (A) The living fibroblasts were exposed to 33 μM propidium iodide, a compound that cannot cross an intact plasma membrane. After incubation for 4 min, the fibroblasts were rinsed with DMEM and imaged 6 min after the first exposure to propidium iodide using (A) DIC images and (B) its fluorescence at 617 nm. Only two cells displayed instability of the membrane. (C) Then, 60 μL of 500 μM Fg-CPP$^{TAT(PTD)}$ was added to the same fibroblasts, yielding a Fg-CPP$^{TAT(PTD)}$ concentration of ~100 μM. The living fibroblasts were imaged 4 min after being exposed to the peptide using its fluorescence at 520 nm. Cells that previously remained free of propidium iodide exhibited uptake of Fg-CPP$^{TAT(PTD)}$. The right panel shows the cell resistance to Fg uptake. (A) Living fibroblasts were exposed to fluorescent marker peptide Fg (20 μM). After incubation for 4 min, cells were imaged using (A) DIC and (B) the fluorescence of FITC at 520 nm. No penetration of Fg into the cells was observed. (C) Then, 30 μL of 200 μM Fg-CPP$^{TAT(PTD)}$ [i.e., the same fluorescent marker peptide Fg, however, this time covalently linked to the cell-penetrating peptide CPP$^{TAT(PTD)}$] was added to the same fibroblasts, yielding a Fg-CPP$^{TAT(PTD)}$ concentration of ~21 μM. Pictures were taken after a 4 min period of contact with the conjugate. Cells that previously remained free of Fg exhibited uptake of Fg-CPP$^{TAT(PTD)}$. Bar = 50 μm.

in the extracellular space (Figure 3B). However, only imaging of the cells immediately after HS addition would display aggregates on the cell membrane in combination with aggregates in the solution (Figure 3B). Thereafter, the aggregates on the membrane disappeared (Figure 1B). In addition, the fluorescence signal in the extracellular fluid became reduced upon addition of HS (Figure 1B) when a HS:Fg-CPP$^{TAT(PTD)}$ molar ratio of ~0.16 was employed. The efficiency of fluorescence quenching and its dependency on

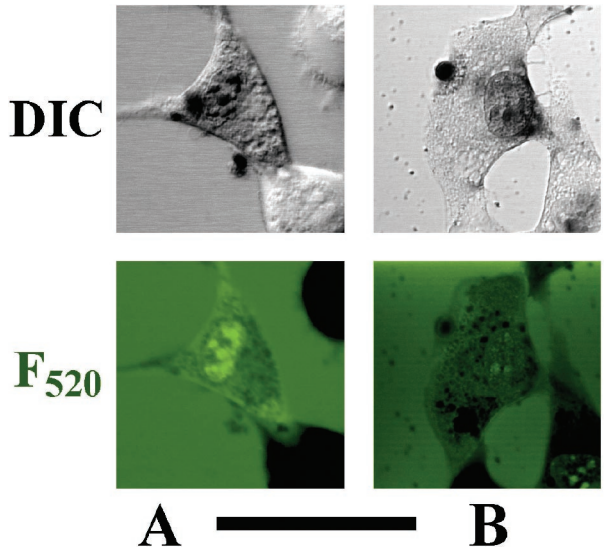

FIGURE 3: Higher magnification of images comparing (A) a normal 4 min exposure to 100 μM Fg-CPP$^{TAT(PTD)}$ and (B) a normal 4 min exposure to Fg-CPP$^{TAT(PTD)}$ followed by addition of HS to the culture chamber for an additional 2 min. (A) Presence of large aggregates with the cell surface contrast with a lack of small aggregates in the extracellular fluid (top) and the same cell showing strong diffuse fluorescence in both the cytoplasm and nucleus (bottom). (B) Presence of small aggregates in the extracellular fluid (top). The lone large aggregate (not displaced by HS addition) provides a hint (top left) of an ingestion to happen. It shows a morphologically modified membrane region under the aggregate that is reminiscent of the organization of coated pits. The slight decrease in extracellular fluorescence results from quenching by the added HS (bottom). The HS:Fg-CPP$^{TAT(PTD)}$ molar ratio ~ 0.04. Bar = 50 μm.

the HS:Fg-CPP$^{TAT(PTD)}$ molar ratio are analyzed in detail below.

Pretreatment of Cells with Heparinase III Reduces the Rate of CPP Uptake and Aggregate Formation. Next, we asked the question of whether the membrane-bound HS might be the possible binding partner for Fg-CPP$^{TAT(PTD)}$. We treated fibroblasts for 1 h with 15 mIU of heparinase III (*31*), an enzyme that degrades the HS chains at the low-sulfation regions of HS (*32*). This treatment significantly reduced the amount of cells labeled with Fg-CPP$^{TAT(PTD)}$ by 32% (Figure 4A,B, left panel; Figure 5A), suggesting that the membrane-associated polysaccharide HS is involved in the uptake mechanism for Fg-CPP$^{TAT(PTD)}$.

Competitive Inhibition of CPP Uptake and Aggregate Formation with Soluble Heparan Sulfate. In Figure 1B, HS was added after an initial CPP uptake. Here, the resulting fluorescence quenching in the extracellular space helped to improve the image contrast for cells that had already incorporated the CPP. On the other hand, when HS was added at the same time as Fg-CPP$^{TAT(PTD)}$, the uptake of the CPP and aggregate formation on the membrane were strongly inhibited (Figure 4, right panel). The extent of reduction was dependent on the HS:Fg-CPP$^{TAT(PTD)}$ molar ratio (Figure 5A). The amount of labeled cells decreased significantly from 46 ± 8% in the absence of HS to 6 ± 5% as the HS:Fg-CPP$^{TAT(PTD)}$ molar ratio increased to 0.16 (Figure 5A).

It is important to note that only those cells incorporated the fluorescent peptide to which aggregates were attached. This spatial coincidence was substantiated by a clear temporal coincidence.

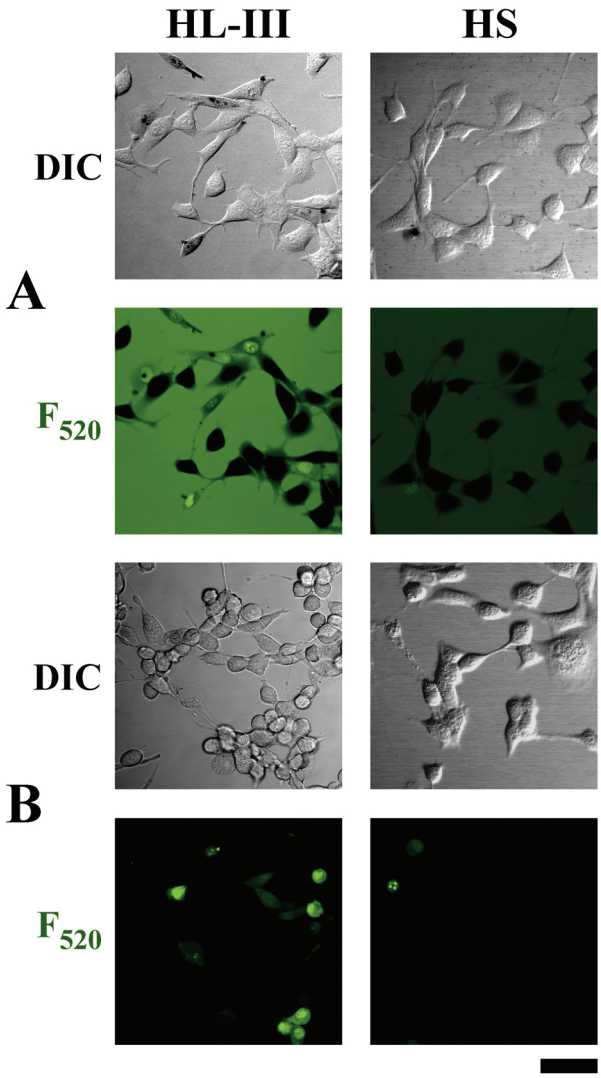

FIGURE 4: Effect of fibroblast pretreatment with heparinase III (left half) and effect of HS added together with the fluorescent peptide (right half). (A) Both procedures [presence of 15 mU of heparinase III for 1 h, or presence of HS at a HS:Fg-CPP$^{TAT(PTD)}$ molar ratio of 0.16] inhibit the formation of aggregates on the cell surface (top). Both procedures decrease the rate of uptake of the fluorescent peptide (bottom). Note that the decrease in intracellular fluorescence caused by HS is associated with a decrease in background fluorescence due to fluorescence quenching. (B) The pretreatment and exposures of fibroblasts were as for panel A, except that, in addition, the peptide-containing medium was removed after the CPP exposure and the fibroblasts were washed with normal culture medium to improve imaging of the decreased intracellular fluorescence. A quantitative summary of these experiments is displayed in Figure 5. Bar = 50 μm.

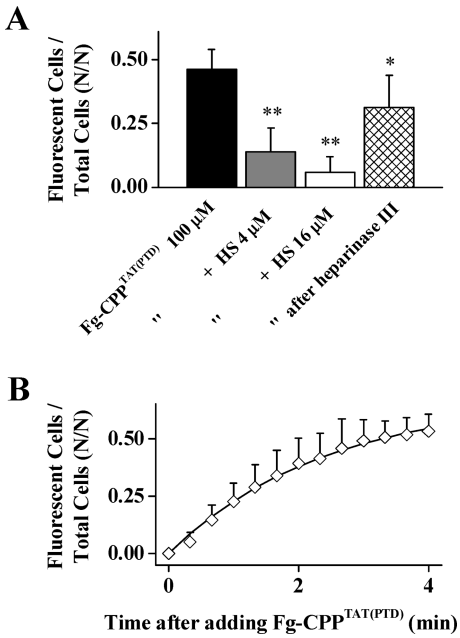

FIGURE 5: Inhibition of CPP uptake and kinetics of CPP uptake (averaged data). (A) In analogy to Figure 4, living fibroblasts were incubated for 4 min with 100 μM Fg-CPP$^{TAT(PTD)}$ and then imaged with confocal fluorescence laser scanning microscopy. The number of cells showing uptake up of Fg-CPP$^{TAT(PTD)}$ (visible in F520) was divided by the total number of cells (visible in DIC). From left to right, the bars denote incubation (i) with Fg-CPP$^{TAT(PTD)}$ only, (ii and iii) in the presence of HS (at two different concentrations), and (iv) after a 1 h treatment with heparinase III. Each bar represents the average of five different cell preparations (mean ± standard deviation, $N = 5$), evaluating four different fields of view (>150 cells) each. One asterisk means $P < 0.05$ vs peptide only. Two asterisks mean $P < 0.001$. (B) Dynamical recordings of CPP uptake (see also Figure 6). The microscopic perfusion chamber (250 μL) contained regular cell culture medium DMEM. At the 0 s time point, 60 μL of 500 μM Fg-CPP$^{TAT(PTD)}$ was added to the fibroblasts, yielding a Fg-CPP$^{TAT(PTD)}$ concentration of ~100 μM. The number of cells that incorporated the peptide (visible in F520) was divided by the total number of cells (visible in DIC), and the ratio is displayed as a function of the period of exposure to Fg-CPP$^{TAT(PTD)}$ (mean ± standard deviation, $N = 11$ cell preparations each at >150 cells evaluated). The mean values were fit (line) with an exponential saturation function, and the fraction of labeled cells = $0.68(1 - e^{-0.41t_{min}})$.

Time Dependence of CPP Uptake and Aggregate Formation. Time-lapse confocal microscopy had an advantage in that the uptake of Fg-CPP$^{TAT(PTD)}$ into nonfixated cells could be monitored in the same cell with a time resolution of 2 s. We observed that the translocation of Fg-CPP$^{TAT(PTD)}$ across the cell membrane started in some fibroblasts as early as 4 s after the administration of the peptide. The percentage of cells with Fg-CPP$^{TAT(PTD)}$ uptake increased with the amount of time they were exposed to Fg-CPP$^{TAT(PTD)}$ (Figure 6), but some cells remained free of Fg-CPP$^{TAT(PTD)}$ even after 4 min, in agreement with earlier reports (*5*, *6*, *23*). The fraction of CPP-labeled cells increased approximately exponentially with time. An exponential fit of Fg-CPP$^{TAT(PTD)}$ uptake (Figure 5B) led to a half-time of ~1.8 min for labeling of the whole cell population, corresponding to a first-order rate constant k of 0.007 s^{-1} at a CPP concentration of ~100 μM. This uptake rate is an agreement with an earlier observation (*33*), but is faster than that reported for a cell-counter assay using a fluorescence quenching test (*23*). In the latter study, the first-order rate constant for the CPP uptake was found to be 0.0003 s^{-1} (*23*). Such differences might be caused by differences in the type of cell strain, the measuring method, or the CPP concentration. There is a remarkable temporal coincidence between cellular CPP uptake and formation of aggregates at the cell surface. Aggregate formation is observed only in cells that take up the peptide, and aggregate formation precedes the CPP uptake by a few seconds (Figure 6). Moreover, the size of the aggregates increases as a function of the amount of time the cells are in contact with Fg-CPP$^{TAT(PTD)}$.

Metabolic Changes Associated with CPP Uptake. Earlier studies reported that 60% of the cells died after contact for 24 h with a 100 μM CPP$^{TAT(PTD)}$ solution (*7*) which is the

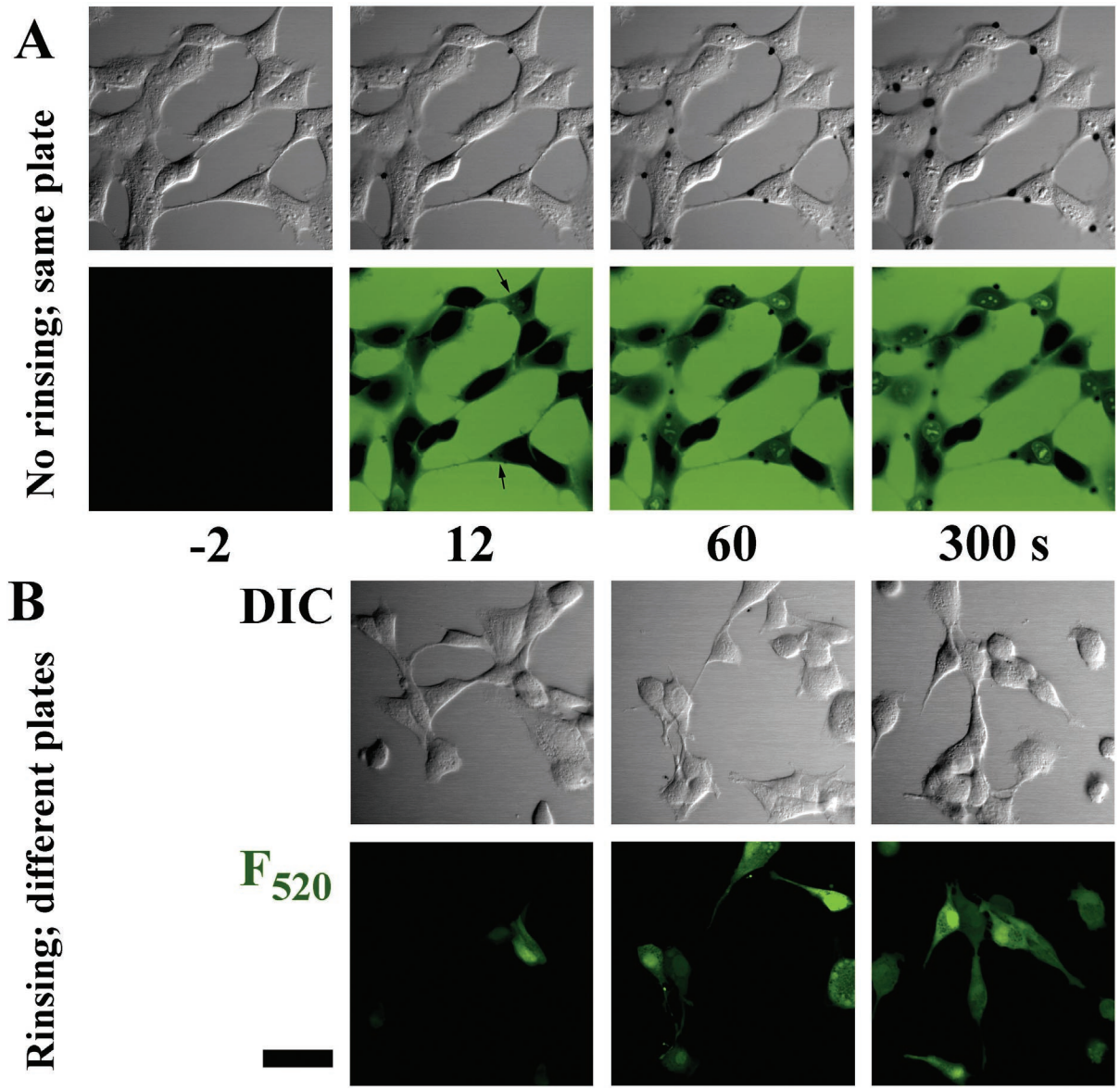

FIGURE 6: Time dependence of CPP uptake. Experimental details as in Figure 5B. (A) The perfusion chamber (250 μL) contained regular cell culture medium DMEM. At the 0 s time point, 60 μL of 500 μM Fg-CPP$^{TAT(PTD)}$ was added to the fibroblasts, yielding a Fg-CPP$^{TAT(PTD)}$ concentration of ~100 μM. Microscopic scans were obtained every 2 s. Some selected views of this series are displayed for the indicated CPP contact time. CPP uptake and formation of aggregates coincide in the same cell only. Arrows indicate that the CPP enters on the side of the cell where the aggregate is found. (B) Living fibroblasts were incubated with 100 μM Fg-CPP$^{TAT(PTD)}$. After the indicated contact time, the cells were rinsed three times with 0.5 mL of regular DMEM to remove the excess fluorescent peptide in the extracellular space, and imaged 2 min later. Intracellular Fg-CPP$^{TAT(PTD)}$ is more visible than in panel A. On the other hand, the spots in the DIC image disappeared. Bar = 50 μm.

same concentration that is used here. We observe that an even shorter contact time (4 min) caused morphological alterations (aggregates) on the cell membrane. These changes appear to be reversible provided the CPP is rapidly washed out (Figure 1C). We therefore investigated whether these apparent morphological alterations caused some functional alterations of fibroblasts. To this purpose, living fibroblasts were studied in real time with a cytosensor microphysiometer, a device commonly used to assess the toxicity of drugs (*27*, *28*). This technique detects minute changes in the proton flux across the cellular membrane. The H^+ flux across the membrane is measured as the so-called extracellular acidification rate (ECAR) and is a sensitive parameter for the functional integrity of living cells (*27*, *28*).

We observed that the CPP$^{TAT(PTD)}$ rapidly reduced the extracellular acidification rate of fibroblasts in a dose-dependent manner (Figure 7, filled bars). The 50 and 500 μM solutions of CPP$^{TAT(PTD)}$ reduced the proton flux by 8 and 22%, respectively. This effect was reversible within 10 min, when the cells [exposed to CPP$^{TAT(PTD)}$ for 2.5 min] were superfused again with medium free of CPP$^{TAT(PTD)}$ (Figure 7, empty bars). In the case of cell necrosis, the ECAR would not have returned to baseline values (*28*). This result clearly demonstrates that short-term exposure to CPP$^{TAT(PTD)}$ does not necessarily cause irreversible damage. However, no recovery to the metabolic baseline was detected when the cells were repeatedly exposed to the elevated CPP$^{TAT(PTD)}$ concentration of 500 μM (data not shown). To test whether the reduction of the ECAR is caused only by the charge or by the specific structure of CPP$^{TAT(PTD)}$, the fibroblasts were superfused with a solution of monomeric arginine, lysine, glycine, glutamine, and tyrosine whose concentrations were

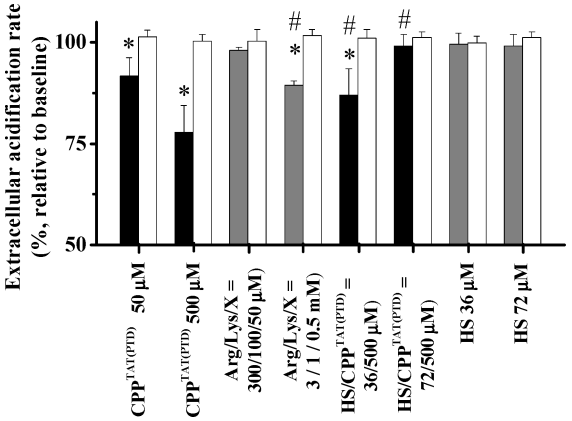

FIGURE 7: Metabolic alterations of fibroblasts during CPP uptake. Approximately 10^6 fibroblasts are perfused with regular cell medium at a rate of 120 μL/min. The rate of the extracellular pH change is recorded every 2 min during a 20 s pump stop using a microphysiometer that measures the extracellular acidification rate (ECAR) of the fibroblasts. Fibroblasts were measured after a 2.5 min exposure to the indicated compounds (shaded bars). The recovery was assessed after subsequent washing with cell culture medium for a period of 2.5 min (empty bars). Data are referenced to baseline ECAR values prior to drug exposure. One asterisk means $P < 0.05$ vs baseline. A pound sign means $P < 0.05$ vs 500 μM $CPP^{TAT(PTD)}$. X is glycine, glutamine, or tyrosine (each at 0.05 or 0.5 mM).

chosen to match the amino acid composition and concentration of the applied $CPP^{TAT(PTD)}$ solution. As seen in Figure 7, the monomeric amino acids have a much less pronounced effect on the ECAR of the fibroblasts, although applied at the same absolute concentrations. In a further experiment, HS was added to the flow medium. The addition of HS inhibited the action of $CPP^{TAT(PTD)}$ on the ECAR (Figure 7) which is consistent with the inhibition of the microscopically observed effects described above. Heparan sulfate alone, however, had no effect on cellular pH regulation (Figure 7).

In Vitro Assessments of Binding Constant, Aggregation, and Fluorescence Quenching. In the study presented here, exogenous HS competitively inhibited (i) CPP uptake, (ii) aggregate formation on the membrane, and (iii) reduction of the ECAR. Hence, we were interested in characterizing the binding thermodynamics between HS and the fluorescent TAT derivative and the efficacy of the observed fluorescence quenching.

Isothermal titration calorimetry revealed that HS binds efficiently to Fg-$CPP^{TAT(PTD)}$ (Figure 8A). The binding constant K_0 [$(4.6 \pm 1.2) \times 10^4$ M^{-1}] is 1 order of magnitude smaller than that reported for the nonfluorescent $CPP^{TAT(PTD)}$ (*29*). This difference is most probably caused by the hydrophobic fluorescent reporter and linker group. The binding is exothermic, and the reaction enthalpy ($\Delta H°$) is -3.60 ± 0.23 kcal/mol of Fg-$CPP^{TAT(PTD)}$ (at 28 °C). The employed HS has a maximum of 6.7 ± 0.4 (n) independent binding sites for Fg-$CPP^{TAT(PTD)}$.

Because Fg-$CPP^{TAT(PTD)}$ has eight positive charges, it can interact simultaneously with several HS molecules, leading to cross-linking and to aggregation. Aggregation was analyzed quantitatively with right-angle light scattering. A titration of Fg-$CPP^{TAT(PTD)}$ with HS is shown in Figure 8B where the scattering intensity is plotted as a function of the HS:Fg-$CPP^{TAT(PTD)}$ ratio. The scattering intensity increases almost linearly up to a HS:Fg-$CPP^{TAT(PTD)}$ ratio of 0.14 ± 0.02 and then decreases slowly again as more HS is added.

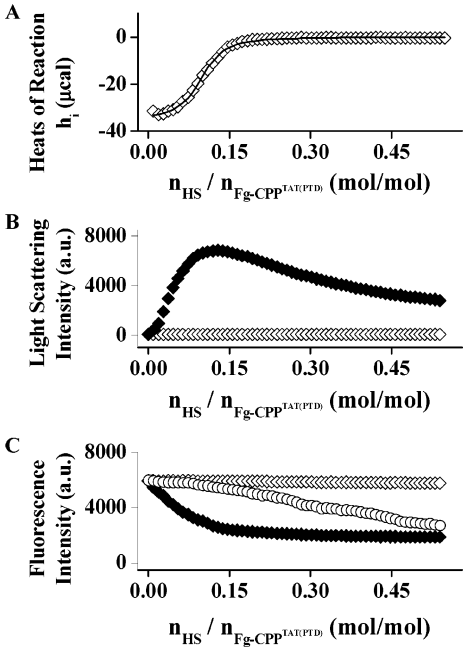

FIGURE 8: Biophysical evidence for binding of HS to Fg-$CPP^{TAT(PTD)}$, aggregation, and fluorescence quenching. (A) Isothermal titration calorimetry. Heat released when 2 μL of 0.50 mM HS is titrated every 5 min (◇) into 78.1 μM Fg-$CPP^{TAT(PTD)}$ at 28 °C. Thermodynamic analysis of the binding isotherm (—) (*29*) yields a reaction enthalpy $\Delta H°$ of -3.60 ± 0.23 kcal/mol of Fg-$CPP^{TAT(PTD)}$, a binding constant K_0 of $(4.6 \pm 1.2) \times 10^4$ M^{-1}, and an n of 6.7 ± 0.4 binding sites (at 28 °C). (B) Right-angle light scattering at 450 nm when 4 μL of 0.10 mM HS (◆) or 4 μL of buffer (◇) is titrated every minute into 2.8 mL of 15.6 μM Fg-$CPP^{TAT(PTD)}$ at 28 °C. (C) Fluorescence quenching of 2.8 mL of 15.6 μM Fg-$CPP^{TAT(PTD)}$ after multiple additions of 4 μL of 100 μM HS (◆), 4 μL of 5.2 mM KI (○), or 4 μL of buffer (◇, dilution control) with constant stirring at 28 °C.

As a control, HS was titrated into pure buffer. No significant light scattering was observed in this titration experiment. The scattering maximum corresponds to a peptide:HS ratio [Fg-$CPP^{TAT(PTD)}$:HS] of $(0.14)^{-1}$ (=7.1), which is in good agreement with isothermal titration calorimetry.

A quenching of the FITC fluorescence was observed during confocal microscopy (Figure 1B), and this quenching was verified by titrating Fg-$CPP^{TAT(PTD)}$ with HS (Figure 8C). Upon addition of HS to Fg-$CPP^{TAT(PTD)}$, the fluorescence intensity was efficiently quenched up to a HS:Fg-$CPP^{TAT(PTD)}$ ratio of 0.14 (Figure 8C), where all the peptide can be expected to be bound according to ITC and light scattering experiments. Thereafter, the addition of HS had only a weak effect on the fluorescence signal. This suggests that the fluorescence quenching was caused by the negative charges of bound HS rather than aggregate formation since the latter is reversed at a higher HS:Fg-$CPP^{TAT(PTD)}$ ratio (Figure 8B). The quenching induced by addition of HS was indeed more efficient than the addition of 0.4 M potassium iodide (Figure 8C), a salt commonly used to quench the fluorescence signal of fluorescent proteins. When the initial:quenched signal ratio (I_0/I) was plotted against the HS concentration, a Stern−Volmer constant (*34*) K_D of 6.8×10^5 M^{-1} of HS was found for the 15.6 μM Fg-$CPP^{TAT(PTD)}$ solution.

DISCUSSION

CPP Uptake Is Not an Artifact of Cell Fixation. The Fg-$CPP^{TAT(PTD)}$ uptake displayed in Figure 6 is the first time-

lapse recording of the uptake of the CPP into living cells. It supports related observation of more than 30 previous studies on chemically fixed cells (for a review, see ref *10*). These earlier studies were recently criticized because chemical fixation potentially damages the cell membrane (*21*, *35*), leading to the leakage of the CPP into the interior of the cell (*21*). In the study presented here, no chemical fixation was required and the living cells incorporated Fg-CPP$^{TAT(PTD)}$ within a very short time (<4 min). The control experiment of Figure 2 also demonstrates that (i) the fluorescent marker dye (Fg) alone does not cross the cell membrane and (ii) the fibroblast membranes were intact when Fg-CPP$^{TAT(PTD)}$ was applied. The integrity of the cellular membrane was confirmed by the exclusion of propidium iodide. The uptake of the CPP through intact membranes is therefore in contrast to a recent report (*36*) in which only cells with defective plasma membranes, as identified by nuclear staining with the ethidium homodimer, showed accumulation of the CPP.

In agreement with earlier studies (*5*, *6*), some cells resisted the entry of the CPP. The percentage of cells with CPP uptake increased, however, with the period of exposure to the CPP (Figure 5B). This study (4 min contact time) and earlier findings (*5*) (8 h contact time) agree that not all cells ingest the CPP. In other studies, a prolonged contact time (>2 h) led to incorporation of the CPP into all cells (*7*, *17*), but also to cell necrosis. Such differences might be caused by different variables and thresholds used to define uptake, by other method-related differences [such as an increased rate of uptake into fixated cells or adsorbed CPPs on the membrane biasing cell counter assays (*35*)], or by cell cycle-dependent differences in HS expression (*37*, *38*) leading to delayed or absent HS uptake (*39*).

Advantage of Confocal Microscopy. Using confocal microscopy makes it possible to distinguish intracellular from extracellular fluorescence without removing the fluorescent peptide from the extracellular medium. Figure 1 shows that the number of labeled cells in the unwashed preparations (Figure 1A) is not different from that after washing with culture medium (Figure 1C). Removal of the extracellular dye improves, however, the contrast because the gain of the photomultiplier can be readjusted to intracellular fluorescence differences.

The distinction between the extracellular and intracellular dye under *in vivo* conditions is possible because of the confocal nature of the images. Specifically, the sampled image plane has a thickness of 0.7 μm which is identical for the extracellular and intracellular space. In contrast, epifluorescence microscopy records the extracellular signal from a much larger volume. Under these conditions, the amount of fluorescent CPP in the extracellular space (sample depth usually of 0.1−1 mm) is much in excess over the amount of the CPP within the fibroblasts (axial cell depth of ∼5 μm). It is for this reason that cells are usually chemically fixed and then trypsinized and washed to remove membrane-bound and extracellular Fg-CPP$^{TAT(PTD)}$, respectively.

Aggregation of Fg-CPP$^{TAT(PTD)}$ with Soluble HS and with Membrane-Bound HS. Using differential interference contrast microscopy, dense aggregates were detected on the surface of the cell membrane. The size of the aggregates increased as a function of the period of contact of the cells with Fg-CPP$^{TAT(PTD)}$ (Figure 6). It is important to note that only those cells which incorporated CPP$^{TAT(PTD)}$ into the cell cytoplasm simultaneously exhibited aggregate formation. Rinsing the cells several times with regular cell medium partially removed these spots (Figure 1C), most likely as a result of a moderate binding constant. The latter may explain why such aggregates have escaped notice in previous studies of rinsed and fixated cells. Another reason could be the specific image contrast used (DIC) or an unfavorable peptide:heparan sulfate ratio in previous studies (i.e., CPP concentrations that were too low).

The aggregate formation *in vivo* is in excellent agreement with the aggregate formation of CPP$^{TAT(PTD)}$ with membrane constituents *in vitro* (*29*). Figure 8B shows that Fg-CPP$^{TAT(PTD)}$ also forms aggregates with soluble HS, with the size of the aggregates and their macroscopic visibility depending strongly on the molar ratio of the two compounds (Figure 8B).

The role of heparan sulfate in aggregate formation and CPP uptake was tested in two different ways. In a first experiment, membrane-bound heparan sulfate was enzymatically removed (at least partially) prior to administration of Fg-CPP$^{TAT(PTD)}$. Treatment of fibroblasts with heparinase III, an enzyme that degrades the HS chains, significantly reduced the number of cells which exhibited CPP uptake (Figure 5A) and aggregate formation (Figure 4, left panel). However, even after heparinase III treatment, a small fraction of cells still incorporated Fg-CPP$^{TAT(PTD)}$, most probably because the enzymatic removal of the glycosaminoglycan chains in living cells was incomplete (*40*) and also because other glycosaminoglycans, such as chondroitin sulfate, could also be involved in peptide uptake and aggregate formation. The latter are not removed with heparinase III treatment. *In vitro* studies have shown that chondroitin sulfate B also binds to CPP$^{TAT(PTD)}$ (*29*).

In a second assay, heparan sulfate was added to the cell medium, competing with the cellular acceptor for the CPP. The outcome of this experiment was strongly dependent on whether heparan sulfate was added after or together with CPP. When exogenous heparan sulfate was added to living fibroblast after the exposure to Fg-CPP$^{TAT(PTD)}$ (Figure 1B), the exogenous HS quenched the extracellular fluorescence but not the intracellular fluorescence so that the Fg-CPP$^{TAT(PTD)}$ in the cell interior could be visualized even better. Under these conditions, aggregates were detected not only on the cell membrane but also, upon magnification, in the extracellular space (Figure 3B). This indicates that the binding of Fg-CPP$^{TAT(PTD)}$ to exogenous HS produces aggregates. These extracellular aggregates have the same image contrast in DIC as those produced by Fg-CPP$^{TAT(PTD)}$ on the cell membrane. The different sizes of the aggregates found on the cell membrane (<5 μm) and those in the extracellular medium (<1 μm) could be caused by the different molar ratios of the compounds (*29*), the time elapsed since the exposure to Fg-CPP$^{TAT(PTD)}$, and the difference in the chemical structure of exogenous and membrane HS. Whereas the externally added, commercial HS had an average molecular mass of 14 200 Da, the HS chains extracted from fibroblasts were found to have a molecular mass of ca. 45 000 Da (*41*). The extent of sulfatation might also be different for the two HS species.

A different result was obtained when HS was added to fibroblasts simultaneously with Fg-CPP$^{TAT(PTD)}$. Under these conditions, both CPP uptake and aggregate formation on the

membrane were strongly inhibited (Figure 4, right panel, and Figure 5A). Exogenous HS may thus act as a competitive inhibitor of both aggregate formation and CPP uptake. The inhibition of CPP uptake is, however, not limited to HS. In an earlier experiment, the cellular uptake of cationic polylysine was inhibited by addition of exogenous heparin (*42*), a natural intracellular compound found in mast cells and chemically closely related to membrane-associated heparan sulfate.

Interestingly, one of the first studies of TAT uptake (*9*) proposed that the uptake mechanism for TAT proceeds via a nonspecific adsorptive endocytosis. In these experiments, a treatment with heparinase could not completely inhibit the TAT uptake, in analogy to our observations. Because of the incomplete inhibition, the authors concluded that glycosaminoglycans were not involved in the uptake mechanism and various alternate uptake mechanisms were proposed (*14*, *43*). In the past 5 years, however, the role of HS has been investigated in more detail and a considerable number of studies now substantiate the important role of heparan sulfate in the uptake of at least $CPP^{TAT(PTD)}$ (*17*−*20*).

Cytotoxicity of $CPP^{TAT(PTD)}$. Prolonged exposure of HeLa cells to TAT at concentrations similar to those employed here has been reported to cause cell necrosis in 60% of the cells after exposure for 24 h (*7*). In the study presented here, even shorter TAT(PTD) exposures (<4 min) lead to functional alterations of living fibroblasts. The cytosensor experiments indicate that the metabolic activity of fibroblasts is significantly disturbed during the exposure to CPP. The fibroblasts responded to the CPP with a fast and dose-dependent reduction of the ECAR which was reversed by superfusing the cells with CPP-free medium. This reduction was specific for the CPP sequence and could not be induced by the corresponding mixture of free amino acids. It could be competitively inhibited with soluble HS. It is unlikely that the reduction of the ECAR is caused by a direct proton exchange with membrane constituents, because the mixture of free amino acids has the same charge as the CPP but does not produce an ECAR reduction. The decrease in the ECAR is probably a direct effect of the CPP on the glycolytic energy metabolism, on proton pumps, or on a shifted proton flux into endosomes (*44*).

In contrast to this reversible reduction of the ECAR after a *short* CPP exposure (<4 min), no recovery to the metabolic baseline was detected in experiments when the cells were repeatedly exposed to an elevated CPP concentration of 500 μM. This result suggests that the CPP can become toxic for fibroblasts depending on the concentration and exposure time. In light of potential medical applications of CPPs, it is also significant that the CPP not only accumulates in the cytosol but also is clearly visible in the nucleus of the fibroblasts (Figures 1−4). The question of whether CPPs can have mutagenic properties, in analogy to the nuclear stain ethidium bromide, thus arises.

Uptake Mechanism. Using intact fibroblasts, we observe a rapid accumulation of the CPP in the cytoplasm and in the nucleus, indicating that the CPP moves with a similar efficiency and rate across the plasma membrane and the nuclear membrane.

The intense fluorescence in the cytoplasm is in agreement with earlier studies (*7*, *45*); however, it is in contrast to a recent study in which the CPP was detected only in the nucleus after a 4 h contact time (8 μM CPP), or in endocytotic vesicles when soluble HS was added (*17*). The different results point to two different uptake mechanisms. The homogeneous distribution of the fluorescent CPP suggests uptake mechanisms such as membrane diffusion (uncharged complex), pores, transporters, etc. In contrast, the localization of the CPP in endocytotic vesicles follows the established endocytotic pathway in which binding of the CPP to the membrane surface induces invagination of the plasma membrane followed by formation of endosomes and subsequent endosome acidification (*45*, *46*). Although endosome acidification might proceed as rapidly (*47*) as the CPP accumulation in the cytoplasm observed here, it has not been observed at temperatures below 11 °C (*48*), a condition under which CPPs are taken up into the cytoplasm (*16*). The two different CPP uptake pathways might coexist where the structure of the CPP could define the proportion of each (*45*, *49*). Fluorescence quenching,[2] wash-out during cell fixation, different contact times (CPP metabolism), and different cell lines could complicate the proper identification of the two pathways (*46*).

In the study presented here, dense aggregates of Fg-$CPP^{TAT(PTD)}$ are formed on the surface of cells which simultaneously show CPP uptake. No aggregates are found on cells which do not exhibit uptake. The cellular and temporal coincidence indicates either that aggregation is part of the uptake mechanism or, alternatively, that aggregation and uptake make use of similar structural and dynamic events in the cell membrane. This study also provides evidence that membrane-bound heparan sulfate plays an important role in this process. The physiologic membrane constituent HS can act as an acceptor for extracellular CPPs and, as such, may lead to peptide uptake at multiple sites of the cell surface. The diffuse fluorescence throughout the cytoplasm and nuclei (Figures 1−3 and 6) suggests an uptake of Fg-$CPP^{TAT(PTD)}$ peptides at numerous sites other than the attachment of aggregates. Those HS−Fg-$CPP^{TAT(PTD)}$ complexes that are not internalized at their site of formation may be laterally transported by membrane movements to aggregates and contribute to their growth. The need for cellular HS in the CPP uptake process is substantiated by a recent knockout model in which no CPP uptake was observed (*19*). Since the HS composition varies as a function of the cell cycle, this may explain why aggregation and CPP uptake can vary within a given cell population.

It is interesting to note that similar observations have been made by other investigators working in fields apparently not related to CPPs. In fact, it has been reported that binding of a ligand to heparan sulfate proteoglycans induces aggregation (*50*) and ligand clustering (*51*, *52*), mediates ligand catabolism (*53*), and stimulates phagocytotic uptake into epithelical cells (*54*). Surface capping of larger aggregates (*55*) and the

[2] The binding of the fluorescent CPP to cellular molecules such as HS led to a substantial fluorescence quenching. Thus, localization and quantification of the CPP in various cellular compartments (including the cell membrane) based on fluorescence intensity might be inappropriate for detecting the complete CPP pathway within the cell. However, the fluorescence quenching might help to reduce the extracellular fluorescence and thus to improve detection of intracellular CPPs in microscopy of living cells. For this purpose, small amounts of HS are added after a first uptake of the CPP. On the other hand, when HS is added simultaneously with CPP, the uptake of CPP is inhibited in a dose-dependent manner.

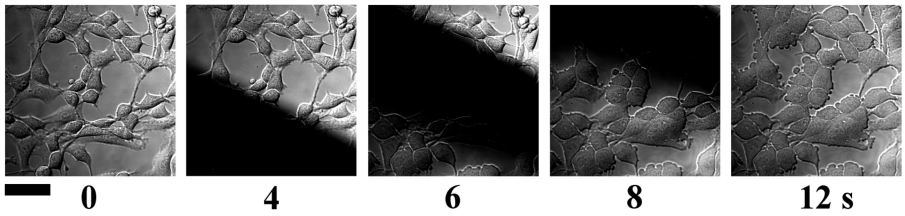

FIGURE 9: Practical considerations of the time dependence of CPP uptake. When Fg-CPP$^{TAT(PTD)}$ was injected into the microscopic infusion chamber, the creation of air bubbles was carefully avoided. These DIC images illustrate the deleterious effect of an air bubble that passes over the fibroblasts located between two glass slides. The front of the air bubble can be recognized by the black front moving from the bottom left to the top right corner in the DIC images (time scale of seconds; bar = 50 μm). The hydrostatic pressure created by the air bubble between the slides is apparently sufficiently high to squeeze the cells. As a result, the fibroblasts present a specific bubbling on the surface which is distinct from the aggregates caused by Fg-CPP$^{TAT(PTD)}$.

assistance of the cytoskeleton (*50*−*52*, *55*) for uptake were observed as well as the transfer to the cell nucleus (*56*, *57*). Some of these phenomena were observed even at 4 °C (*50*) and are therefore very similar to the reported temperature independence of TAT uptake (*4*, *7*, *14*, *16*) and polylysine uptake (*2*). The aggregation of HS and the subsequent uptake are considered to be different from classical endocytosis because it occurs without the formation of coated pits (*53*). Since these studies used antibodies against HS and its proteoglycans (HSPGs) to induce aggregation, they were only negligibly noticed in CPP research. In light of recent (*29*) and our experiments, however, it seems that CPP aggregation with HS acts in a similar way, and causes an even more effective aggregation and faster uptake than aggregation with antibodies.

In summary, the involvement of HS in the CPP uptake mechanism is evidenced by the following. (i) Enzymatic removal of membrane-associated HS chains reduces the rate of both CPP uptake and aggregate formation. (ii) The co-administration of exogenous HS competitively inhibits three cellular effects: the CPP uptake itself, the formation of aggregates on the cell membrane, and the reduction of the ECAR. (iii) The DIC image contrast of these aggregates on the membrane could be mimicked with a source of binding of exogenous heparan sulfate to the CPP. The involvement of HS in the CPP uptake is in further agreement with recent *in vivo* findings in which cells with a defect in the HS biosynthesis exhibited an impaired TAT internalization (*19*).

APPENDIX

For the study of the time dependence of the CPP uptake (Figures 5B and 6), the Fg-CPP$^{TAT(PTD)}$ was injected into a microscopic infusion chamber and microscopic scans were obtained every 2 s. During this injection, the creation of air bubbles was carefully avoided. Figure 9 illustrates the deleterious effect of an air bubble that passes over the fibroblasts located between the two glass slides separated by 1 mm. The front of the air bubble can be easily recognized by the large black front moving from the bottom left to the top right corner in the DIC images. The hydrostatic pressure created by the air bubble between the glass slides is apparently sufficiently high to squeeze the cells. As a result, the fibroblasts present a specific bubbling on the cell surface which is distinct from the aggregates caused by the Fg-CPP$^{TAT(PTD)}$ (Figures 1−6). This bubbling effect is most pronounced for cells that are not spread on the slides, but that are lifted from the glass plate as a part of the fibroblasts' replication cycle. The morphological changes caused by the air bubble (between slides) are also distinct from the simple contact to air, because removing the cell culture medium on a single glass plate could not produce such an effect (result not shown).

REFERENCES

1. Ryser, H. J., and Hancock, R. (1965) Histones and basic polyamino acids stimulate the uptake of albumin by tumor cells in culture, *Science 150*, 501−503.
2. Ryser, H. J. (1968) Uptake of protein by mammalian cells: An underdeveloped area. The penetration of foreign proteins into mammalian cells can be measured and their functions explored, *Science 159*, 390−396.
3. Shen, W. C., and Ryser, H. J. (1978) Conjugation of poly-L-lysine to albumin and horseradish peroxidase: A novel method of enhancing the cellular uptake of proteins, *Proc. Natl. Acad. Sci. U.S.A. 75*, 1872−1876.
4. Mitchell, D. J., Kim, D. T., Steinman, L., Fathman, C. G., and Rothbard, J. B. (2000) Polyarginine enters cells more efficiently than other polycationic homopolymers, *J. Pept. Res. 56*, 318−325.
5. Green, M., and Loewenstein, P. M. (1988) Autonomous functional domains of chemically synthesized human immunodeficiency virus tat trans-activator protein, *Cell 55*, 1179−1188.
6. Frankel, A. D., and Pabo, C. O. (1988) Cellular uptake of the tat protein from human immunodeficiency virus, *Cell 55*, 1189−1193.
7. Vives, E., Brodin, P., and Lebleu, B. (1997) A truncated HIV-1 Tat protein basic domain rapidly translocates through the plasma membrane and accumulates in the cell nucleus, *J. Biol. Chem. 272*, 16010−16017.
8. Fawell, S., Seery, J., Daikh, Y., Moore, C., Chen, L. L., Pepinsky, B., and Barsoum, J. (1994) Tat-Mediated Delivery of Heterologous Proteins into Cells, *Proc. Natl. Acad. Sci. U.S.A. 91*, 664−668.
9. Mann, D. A., and Frankel, A. D. (1991) Endocytosis and targeting of exogenous HIV-1 Tat protein, *EMBO J. 10*, 1733−1739.
10. Schwarze, S. R., Hruska, K. A., and Dowdy, S. F. (2000) Protein transduction: Unrestricted delivery into all cells? *Trends Cell Biol. 10*, 290−295.
11. Lindgren, M., Hallbrink, M., Prochiantz, A., and Langel, U. (2000) Cell-penetrating peptides, *Trends Pharmacol. Sci. 21*, 99−103.
12. Derossi, D., Chassaing, G., and Prochiantz, A. (1998) Trojan peptides: The penetratin system for intracellular delivery, *Trends Cell Biol. 8*, 84−87.
13. Silhol, M., Tyagi, M., Giacca, M., Lebleu, B., and Vives, E. (2002) Different mechanisms for cellular internalization of the HIV-1 Tat-derived cell penetrating peptide and recombinant proteins fused to Tat, *Eur. J. Biochem. 269*, 494−501.
14. Derossi, D., Calvet, S., Trembleau, A., Brunissen, A., Chassaing, G., and Prochiantz, A. (1996) Cell internalization of the third helix of the Antennapedia homeodomain is receptor-independent, *J. Biol. Chem. 271*, 18188−18193.
15. Wender, P. A., Mitchell, D. J., Pattabiraman, K., Pelkey, E. T., Steinman, L., and Rothbard, J. B. (2000) The design, synthesis, and evaluation of molecules that enable or enhance cellular uptake: Peptoid molecular transporters, *Proc. Natl. Acad. Sci. U.S.A. 97*, 13003−13008.
16. Futaki, S., Suzuki, T., Ohashi, W., Yagami, T., Tanaka, S., Ueda, K., and Sugiura, Y. (2001) Arginine-rich peptides. An abundant

source of membrane-permeable peptides having potential as carriers for intracellular protein delivery, *J. Biol. Chem. 276*, 5836−5840.
17. Sandgren, S., Cheng, F., and Belting, M. (2002) Nuclear targeting of macromolecular polyanions by an HIV-Tat derived peptide. Role for cell-surface proteoglycans, *J. Biol. Chem. 277*, 38877−38883.
18. Rusnati, M., Coltrini, D., Oreste, P., Zoppetti, G., Albini, A., Noonan, D., d'Adda di Fagagna, F., Giacca, M., and Presta, M. (1997) Interaction of HIV-1 Tat protein with heparin. Role of the backbone structure, sulfation, and size, *J. Biol. Chem. 272*, 11313−11320.
19. Tyagi, M., Rusnati, M., Presta, M., and Giacca, M. (2001) Internalization of HIV-1 tat requires cell surface heparan sulfate proteoglycans, *J. Biol. Chem. 276*, 3254−3261.
20. Belting, M. (2003) Heparan sulfate proteoglycan as a plasma membrane carrier, *Trends Biochem. Sci. 28*, 145−151.
21. Lundberg, M., and Johansson, M. (2001) Is VP22 nuclear homing an artifact? *Nat. Biotechnol. 19*, 713.
22. Nath, A., Psooy, K., Martin, C., Knudsen, B., Magnuson, D. S. K., Haughey, N., and Geiger, J. D. (1996) Identification of a human immunodeficiency virus type 1 tat epitope that is neuroexcitatory and neurotoxic, *J. Virol. 70*, 1475−1480.
23. Hallbrink, M., Floren, A., Elmquist, A., Pooga, M., Bartfai, T., and Langel, U. (2001) Cargo delivery kinetics of cell-penetrating peptides, *Biochim. Biophys. Acta 1515*, 101−109.
24. Ziegler, A., Blatter, X. L., Seelig, A., and Seelig, J. (2003) Protein transduction domains of HIV-1 and SIV TAT interact with charged lipid vesicles. Binding mechanism and thermodynamic analysis, *Biochemistry 42*, 9185−9194.
25. Ho, A., Schwarze, S. R., Mermelstein, S. J., Waksman, G., and Dowdy, S. F. (2001) Synthetic protein transduction domains: Enhanced transduction potential in vitro and in vivo, *Cancer Res. 61*, 474−477.
26. Griffin, C. C., Linhardt, R. J., Van Gorp, C. L., Toida, T., Hileman, R. E., Schubert, R. L., II, and Brown, S. E. (1995) Isolation and characterization of heparan sulfate from crude porcine intestinal mucosal peptidoglycan heparin, *Carbohydr. Res. 276*, 183−197.
27. Landwojtowicz, E., Nervi, P., and Seelig, A. (2002) Real-time monitoring of P-glycoprotein activation in living cells, *Biochemistry 41*, 8050−8057.
28. McConnell, H. M., Owicki, J. C., Parce, J. W., Miller, D. L., Baxter, G. T., Wada, H. G., and Pitchford, S. (1992) The cytosensor microphysiometer: Biological applications of silicon technology, *Science 257*, 1906−1912.
29. Ziegler, A., and Seelig, J. (2004) Interaction of the Protein Transduction Domain of HIV-1 TAT with Heparan Sulfate: Binding mechanism and thermodynamic parameters, *Biophys. J. 86*, 254−263.
30. Nomarski, G. (1955) Microinterferometric differential a l'ondes polarisees, *J. Radiat. Phys. 16*, 9−135.
31. Suzuki, T., Futaki, S., Niwa, M., Tanaka, S., Ueda, K., and Sugiura, Y. (2002) Possible existence of common internalization mechanisms among arginine-rich peptides, *J. Biol. Chem. 277*, 2437−2443.
32. Linhardt, R. J., Turnbull, J. E., Wang, H. M., Loganathan, D., and Gallagher, J. T. (1990) Examination of the substrate specificity of heparin and heparan sulfate lyases, *Biochem. J. 29*, 2611−2617.
33. Nagahara, H., Vocero-Akbani, A. M., Snyder, E. L., Ho, A., Latham, D. G., Lissy, N. A., Becker-Hapak, M., Ezhevsky, S. A., and Dowdy, S. F. (1998) Transduction of full-length TAT fusion proteins into mammalian cells: TAT-p27Kip1 induces cell migration, *Nat. Med. 4*, 1449−1452.
34. Eftnik, M. R., and Ghiron, C. A. (1981) Fluorescence Quenching Studies with Proteins, *Anal. Biochem. 114*, 199−227.
35. Richard, J. P., Melikov, K., Vives, E., Ramos, C., Verbeure, B., Gait, M. J., Chernomordik, L. V., and Lebleu, B. (2003) Cell-penetrating peptides. A reevaluation of the mechanism of cellular uptake, *J. Biol. Chem. 278*, 585−590.
36. Kramer, S. D., and Wunderli-Allenspach, H. (2003) No entry for TAT(44−57) into liposomes and intact MDCK cells: Novel approach to study membrane permeation of cell-penetrating peptides, *Biochim. Biophys. Acta 1609*, 161−169.
37. Kraemer, P. M., and Tobey, R. A. (1972) Cell-cycle dependent desquamation of heparan sulfate from the cell surface, *J. Cell Biol. 55*, 713−717.
38. Fedarko, N. S., and Conrad, H. E. (1986) A unique heparan sulfate in the nuclei of hepatocytes: Structural changes with the growth state of the cells, *J. Cell Biol. 102*, 587−599.
39. Fedarko, N. S., Ishihara, M., and Conrad, H. E. (1989) Control of cell division in hepatoma cells by exogenous heparan sulfate proteoglycan, *J. Cell. Physiol. 139*, 287−294.
40. Schulz, J. G., Megow, D., Reszka, R., Villringer, A., Einhaupl, K. M., and Dirnagl, U. (1998) Evidence that glypican is a receptor mediating β-amyloid neurotoxicity in PC12 cells, *Eur. J. Neurosci. 10*, 2085−2093.
41. Turnbull, J. E., and Gallagher, J. T. (1991) Distribution of iduronate 2-sulphate residues in heparan sulphate. Evidence for an ordered polymeric structure, *Biochem. J. 273* (Part 3), 553−559.
42. Morad, N., Ryser, H. J., and Shen, W. C. (1984) Binding sites and endocytosis of heparin and polylysine are changed when the two molecules are given as a complex to Chinese hamster ovary cells, *Biochim. Biophys. Acta 801*, 117−126.
43. Prochiantz, A. (2000) Messenger proteins: Homeoproteins, TAT and others, *Curr. Opin. Cell Biol. 12*, 400−406.
44. Van Dyke, R. W. (1995) Na^+/H^+ exchange modulates acidification of early rat liver endocytic vesicles, *Am. J. Physiol. 269*, C943−C954.
45. Potocky, T. B., Menon, A. K., and Gellman, S. H. (2003) Cytoplasmic and nuclear delivery of a TAT-derived peptide and a β-peptide after endocytic uptake into HeLa cells, *J. Biol. Chem. 278*, 50188−50194.
46. Fischer, R., Kohler, K., Fotin-Mleczek, M., and Brock, R. (2004) A stepwise dissection of the intracellular fate of cationic cell-penetrating peptides, *J. Biol. Chem. 279*, 12625−12635.
47. Maxfield, F. R., and Yamashiro, D. J. (1987) Endosome acidification and the pathways of receptor-mediated endocytosis, *Adv. Exp. Med. Biol. 225*, 189−198.
48. Roederer, M., Bowser, R., and Murphy, R. F. (1987) Kinetics and temperature dependence of exposure of endocytosed material to proteolytic enzymes and low pH: Evidence for a maturation model for the formation of lysosomes, *J. Cell. Physiol. 131*, 200−209.
49. Zaro, J. L., and Shen, W. C. (2003) Quantitative comparison of membrane transduction and endocytosis of oligopeptides, *Biochem. Biophys. Res. Commun. 307*, 241−247.
50. Martinho, R. G., Castel, S., Urena, J., FernandezBorja, M., Makiya, R., Olivercrona, G., Reina, M., Alonso, A., and Vilaro, S. (1996) Ligand binding to heparan sulfate proteoglycans induces their aggregation and distribution along actin cytoskeleton, *Mol. Biol. Cell 7*, 1771−1788.
51. Carey, D. J., Stahl, R. C., Tucker, B., Bendt, K. A., and Cizmecismith, G. (1994) Aggregation-Induced Association of Syndecan-1 with Microfilaments Mediated by the Cytoplasmic Domain, *Exp. Cell Res. 214*, 12−21.
52. Fuki, I. V., Meyer, M. E., and Williams, K. J. (2000) Transmembrane and cytoplasmic domains of syndecan mediate a multi-step endocytic pathway involving detergent-insoluble membrane rafts, *Biochem. J. 351* (Part 3), 607−612.
53. Williams, K. J., and Fuki, I. V. (1997) Cell-surface heparan sulfate proteoglycans: Dynamic molecules mediating ligand catabolism, *Curr. Opin. Lipidol. 8*, 253−262.
54. Dehio, C., Freissler, E., Lanz, C., Gomez-Duarte, O. G., David, G., and Meyer, T. F. (1998) Ligation of cell surface heparan sulfate proteoglycans by antibody-coated beads stimulates phagocytic uptake into epithelial cells: A model for cellular invasion by *Neisseria gonorrhoeae*, *Exp. Cell Res. 242*, 528−539.
55. Bretscher, M. S. (1996) Getting membrane flow and the cytoskeleton to cooperate in moving cells, *Cell 87*, 601−606.
56. Tumova, S., Hatch, B. A., Law, D. J., and Bame, K. J. (1999) Basic fibroblast growth factor does not prevent heparan sulphate proteoglycan catabolism in intact cells, but it alters the distribution of the glycosaminoglycan degradation products, *Biochem. J. 337* (Part 3), 471−481.
57. Ishihara, M., Fedarko, N. S., and Conrad, H. E. (1986) Transport of heparan sulfate into the nuclei of hepatocytes, *J. Biol. Chem. 261*, 13575−13580.

BI0491604